

LANE 2010

## In-Situ Quality Monitoring During Laser Brazing

Michael Ungers<sup>1</sup>, Daniel Fecker<sup>2</sup>, Sascha Frank<sup>3</sup>, Dmitri Donst<sup>3</sup>, Volker Märgner<sup>2</sup>, Peter Abels<sup>1</sup>, Stefan Kaielerle<sup>1\*</sup>

<sup>1</sup>Fraunhofer Institute for Laser Technology ILT, Aachen, Steinbachstrasse 15, 52074 Aachen, Germany

<sup>2</sup>Institute for Communications Technology IfN, TU Braunschweig, Schleinitzstrasse 22, 38106 Braunschweig, Germany

<sup>3</sup>Fraunhofer Institute for Production Technology IPT, Aachen, Steinbachstrasse 17, 25074 Aachen, Germany

---

### Abstract

Laser brazing of zinc coated steel is a widely established manufacturing process in the automotive sector, where high quality requirements must be fulfilled. The strength, impermeability and surface appearance of the joint are particularly important for judging its quality. The development of an on-line quality control system is highly desired by the industry. This paper presents recent works on the development of such a system, which consists of two cameras operating in different spectral ranges. For the evaluation of the system, seam imperfections are created artificially during experiments. Finally image processing algorithms for monitoring process parameters based the captured images are presented.

*Keywords:* On-line quality control; laser brazing; process sensing and controlling; process optimisation; process monitoring

---

### 1. Introduction

Today, laser brazing is becoming a well established laser joining technique that is fully integrated in industrial production lines. Due to narrow seams combined with high strength and smooth surfaces this thermal joining technique offers efficient and attractive solutions to the automotive sector. For example, the joining of chassis components requires high standards concerning the strength and reliability. Moreover a good optical appearance of the joint is highly desired, as these joints are often placed in visible regions of the vehicle. Therefore, quality control must not be neglected. For controlling the quality of brazed seams several systems are currently commercially available, e.g. a quality control system developed by Müßigmann et. al. [1]. This system uses image processing algorithms to detect pores automatically in a brazed seam. A comparable approach is shown by Müller-Borhanian et. al. [2]. Here the principle of triangulation is used to control the quality of the joint. But all these systems operate in a post process configuration. To avoid these time and cost consuming off-line inspections and to enhance the

---

\* Corresponding author: Michael Ungers Tel.: +49 (0) 8906 281; fax: +49 (0) 8906 121.  
E-mail address: [michael.ungers@ilt.fraunhofer.de](mailto:michael.ungers@ilt.fraunhofer.de).

efficiency of the quality control, the development of an on-line quality control system is highly desired by the industry. Grimm and Schmidt [3] describe a way of online monitoring with two cameras mounted off-axis. Hence, the setup is more in a laboratory stage and is not applicable for the industry, yet.

In contrast, this paper presents the current works on the development of an online quality control system. The goal is to measure different process parameters as well as seam imperfections and defects in an online configuration that is adaptable for standard brazing applications. Therefore an approach is chosen that consists of two cameras observing the process simultaneously in different spectral ranges. To detect more than just the radiation emitted by the process an external illumination is included.

In the following three different stages of the development are illustrated. In section 2 the process is analyzed and seam imperfections are classified. In particular the emergence process of different defects is investigated. Based on this knowledge experiments are carried out to develop and evaluate the optical system, which is described in section 3. In section 4 the implementation of image processing algorithms is presented. Finally the results are summarized in a conclusion and a short outlook for the next stages of the development is given.

## 2. Classification and analysis of seam imperfections

In order to create an online quality control system for the detection of imperfections and defects in brazed joints, these imperfections first need to be defined. To efficiently test this system, one also needs to be able to create seam imperfections tentatively. This requires research on the formation mechanisms of these imperfections, especially since some imperfections, e.g. pores, do not occur systematically but sporadically. A deeper understanding of the mechanisms related to the occurrence of seam imperfections also supports the development and selection of criteria suitable for the detection of these phenomena. Thus, the research into these formation mechanisms directly contributes to the development of the quality control system.

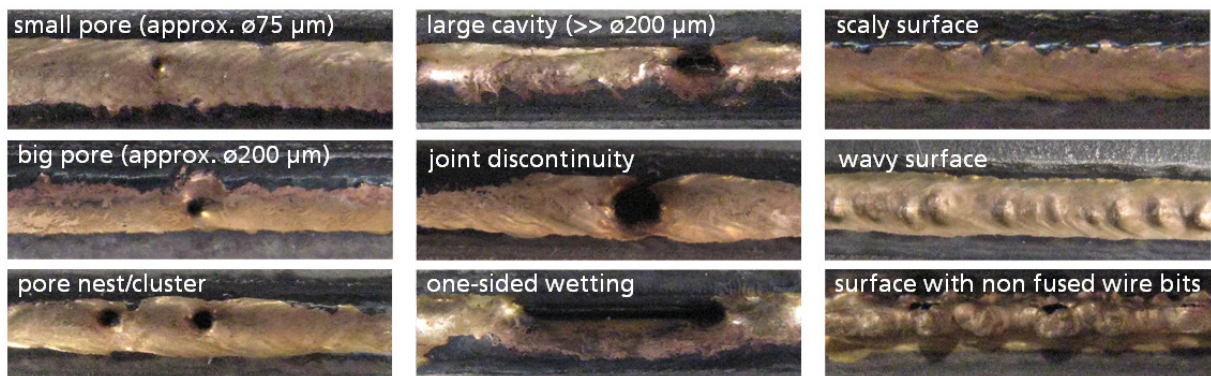


Figure 1: Different types and varieties of geometrical seam imperfections [5]

Consequently, a large number of experiments were conducted and evaluated by Fraunhofer IPT with the objective of categorizing various seam imperfections and researching their formation mechanisms. The process parameters that were varied in these experiments include the orientation of wire feed, laser spot and workpiece, laser output power and brazing speed. In accordance with the project specifications and industry needs, these experiments focused on brazing zinc coated steel using copper based filler wire. The analysis of the data generated in these experiments revealed three different basic types of seam imperfections, which may appear in various sizes and intensities and are shown in Fig. 1. In detail, the three types can be described as follows:

- Pores of sporadic occurrence, including small pores, big pores and pore clusters (1<sup>st</sup> column of Fig. 1).
- Joint disruptions in the shape of large cavities, joint discontinuities and one-sided wetting (2<sup>nd</sup> column of Fig. 1).
- Surface irregularities in the form of scaly or wavy seam surfaces, also including surfaces with protruding bits of non fused brazing wire (3<sup>rd</sup> column of Fig. 1).

The imperfections listed above can be classified as imperfections of the seam geometry. Additionally, it was possible to identify imperfections which affect the surface appearance of the seam without necessarily having a significant influence on its geometry. In general, these kinds of imperfections are connected to the metallurgical composition of the joint. Fig. 2 shows two examples of these metallurgical imperfections in direct comparison to a seam with good surface quality (1<sup>st</sup> column). The first imperfection, shown in the centre column of Fig. 2, appears in the shape of a jagged black line that continues along the seam surface. First analyses indicate, that this imperfection may be caused by the separation and oxidation of the alloying elements contained in the filler material. This process is affected by the intensity of the melt pool movements. It is yet unclear, how strongly this anomaly influences the mechanical properties of the brazed joint and the adhesion of possible surface coatings. The third column of Fig. 2 shows a seam that is strongly affected by a partial melting of the base material. Melting the base material on a macroscopic scale is usually not desired as part of a brazing process, as stated by Humpston et. al. [4]. It may have a negative effect on the mechanical and chemical properties of the joint as well as its surface appearance. Thus, a partial melting of the base material can also be classified as a seam imperfection. As shown by the cross-sectional detail views in the second row of Fig. 2, these imperfections have very little influence on the seam surface geometry.

The oxidation together with the partial melting of the base material can be summarised as a metallurgical seam imperfection. Together with the three types listed above, four types of seam imperfections are now defined.

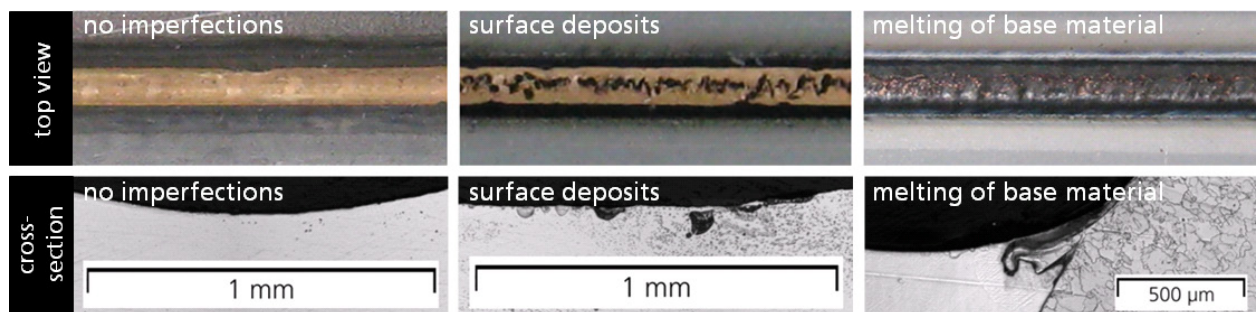


Figure 2: Seam surfaces affected by different metallurgical effects

Brazing is frequently utilized in industrial applications where smooth joint surfaces are required. For this reason, mainly seam imperfections which affect the seam surface were investigated. Accordingly, all of the pores which were investigated are surface pores and match the type commonly referred to as »worm holes«. These types of pores permeate the whole seam in a direction roughly vertical to the surface. In automotive applications, the quality requirements are quite high and even small pores in visible areas need to be reworked if their diameter exceeds 200 µm, as stated by Müller-Borhanian et. al. [2]. Due to their sporadic occurrence, pores are also especially difficult to avoid or predict. The reliable detection of pores is thus of particular interest to the industry. Consequently, the formation mechanisms of pores are being investigated extensively as part of the development of the quality control system.

### 2.1. Pore formation: State of the art

The formation of pores has been investigated by various groups, which came to different conclusions regarding the causes of pore formation. These sources have previously been presented and discussed by Donst et. al. [5]. In addition, some recent publications have provided more detailed analyses of the actual process of pore formation. One such description is given by Kimura et. al. [6]. This group states that the process of pore formation is initiated by a wetting irregularity, which may be caused by escaping zinc vapour. According to the images provided, this irregularity originates in the area where the initial wetting of the joining partners takes place. The wetting irregularity is then enclosed by the melt pool without closing completely. It is concluded that the resulting pore remains open due to the high vapour pressure of zinc and a low wire feed rate. This mechanism was only observed at low wire feed rates.

Similar observations regarding pore formation were made by Grimm and Schmidt [3]. Here, oscillations in the melt pool are observed during the brazing process, which are assumed to be based on melting and solution effects. A

partial necking of the melt pool happens when these oscillations are disturbed, leading to a gap between melt pool and workpiece. It is inferred that these disturbances in the melt pool oscillation occur due to a lateral or vertical misalignment of the joining partners, laser spot and brazing wire. According to this group, the gap between melt pool and workpiece remains open due to gas jets of zinc vapour. The gap then leads to the formation of either a pore or a joint disruption. It is also stated that pores originating at one of the joining partners may continue to drift into the middle of the seam before solidifying.

## 2.2. Pore formation: Analysis results

Due to the inconsistent nature of the conclusions drawn by other sources, an in depth analysis of pore formation was conducted using a high speed camera capable of recording images at rates in excess of 10,000 fps. In consistence with the observations made by Grimm and Schmidt [3], an oscillation of the melt pool could be observed in the high speed recordings. The recordings also show a correlation between these oscillations and an irregular movement of the brazing wire entering the melt pool. This irregular wire movement has mainly been attributed to the slip stick effect by Donst et. al. [5]. It has also been observed to be a source of pore formation. Fig. 3 illustrates the mechanism of pore formation due to an irregular wire feed rate, broken down into three different steps.

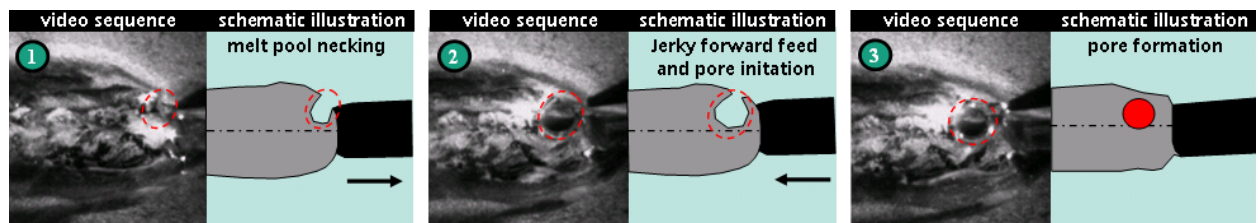


Figure 3: Mechanism of pore formation

In step 1, the brazing wire is pulled back from the melt pool due to the irregular feed rate, interrupting the previously stable brazing process. The irregular motion of the wire leads to an unsteady supply of liquid braze, causing the formation of a neck in the melt pool in the area where the wetting of the joining partners takes place. In the given example, the neck of the melt pool is shaped irregularly and causes a one sided indentation to form in the melt, which is marked in the image. This could also be described as the temporary occurrence of one sided wetting. In step 2, the wire starts to move forward again, initiating a pore by enclosing the cavity in the melt. Step 3 shows the final stage of pore formation, where the pore is enclosed by the melt on all sides and the steady brazing process continues. Once the formation process is completed, the pores tend to drift towards the centre of the melt. A detailed look at pore drifting and solidification has already been presented by Donst et. al. [5]. As stated here, zinc vapour permeating the melt pool could not be confirmed as a major cause for the formation of worm hole pores.

Despite the analysis of the mechanisms provided above, the occurrence of pores still happens sporadically and cannot be predicted. On the other hand, the process irregularities leading to the formation of pores may be intensified by external influences. For example, the misalignment of brazing wire and laser beam to the joint has been observed to increase the likeliness of wetting irregularities, resulting in a larger amount of pores. Furthermore, pores have been observed to occur more frequently when the wire feed rate is lower than the brazing speed. An increased amount of pores could also be observed during experiments performed with a wire feeding nozzle of unsuitable diameter. Since the diameter of the nozzle was chosen too large, the wire tip was permitted a much larger freedom of movement than usually intended. This led to an increased number of seam imperfections, including pores. The conditions leading to increased pore occurrences may be summarized as follows:

- Unsteady relation of wire feed and brazing speed
- Misalignment of wire, laser spot and joining partners in lateral and/or vertical direction
- Low wire feed rates
- Unsteady wire movement in lateral and/or vertical direction, e.g. due to a large diameter wire nozzle

The steps of the pore formation mechanism described above largely match those reported by Kimora et. al. [6] and by Grimm and Schmidt [3]. In all three cases, the pores were observed to originate from the same critical area, in which melt pool and work piece first come into contact. A neck is formed and consequently surrounded by the melt to form a pore. However, the groups disagree on the possible causes leading to an initiation of the pore formation mechanism.

According to the process analysis conducted by Fraunhofer IPT, the formation of pores is initiated when a process irregularity disturbs the melt pool dynamics in such a way that the steady wetting of the base material is interrupted. While different groups attribute the initiation of the pore forming procedure to different causes, all agree on the fact that an external influence is required to trigger a pore forming event. By implication, this means that there is no intrinsic reason which causes pores to originate from the melt pool dynamics themselves. Pores are only generated when other elements of the brazing process, like an irregular wire feed rate, interrupt the stable interaction between liquid braze and workpiece by enacting an external influence on them. One such external trigger event that could be confirmed through observation is an irregular wire movement, as illustrated in Fig. 3. Irregular movements of the wire which trigger the formation of pores may also happen in the lateral or vertical direction. Another such trigger event that has been proposed by several groups, yet could not be confirmed through observation, is the influence of zinc vapour on the melt pool dynamics.

The process conditions listed above that lead to an increased frequency of pore forming events do so by either causing an increased number of trigger events or by making the process more susceptible to such trigger events. For example, a lateral misalignment of the joining partners towards laser spot and feeding wire will encumber the wetting process on the side of the joint which is farther removed from the wire, making it more susceptible towards events disturbing the wetting process on this side. Using a larger wire nozzle, on the other hand, will lead to an irregular movement of the wire tip by granting it a larger freedom of movement, thus generating more process irregularities that may initiate the formation of pores.

For the purpose of testing the online quality monitoring system, the results of this analysis were used to artificially generate increased amounts of pores. Similar approaches were taken to develop detection methods for the other types of imperfections described in section 2. The optical system used to monitor the process will be described in detail in the next section.

### **3. The optical system**

To achieve a good adaptability for standard issued laser applications the concept of the CPC-System is chosen (Coaxial-Process-Control). Due to its coaxial implementation into the optical path of the processing laser, there are no limitations regarding the movement of the laser head. Curved seams and even 3D-applications can be joined without any directional limitations caused by external cameras or measurement equipment. A complete overview concerning the CPC-System, developed by Fraunhofer ILT, and the process observation approaches related to it, are introduced by Kaieler et. al. in [7] and [8].

#### *3.1. General description of the optical system*

The principal idea of the quality control system is shown in Fig. 4 (a). It consists of two cameras – a high-speed CMOS (Complementary Metal Oxide Semiconductor) camera and a NIR (Near Infra-Red) camera – observing the process in a coaxial arrangement. Two beam splitters are used for the coaxial integration of the cameras into the optical path of the Nd:YAG laser. In addition to the two cameras an external illumination is applied coaxial to the path of the brazing laser to illuminate the whole process zone for capturing images with the CMOS camera. This hardware configuration enables the simultaneous analysis of real images of the process, showing the geometrical dimensions, as well as images of the thermal radiation, showing the heat distribution in the sample. Process parameters and emerging seam imperfections can be resolved with high temporal and spatial accuracy. The realised experimental setup is shown in Fig. 4 (b). An overview of the specific camera parameters is given in Table 1.

Table 1: Overview of the camera specifications

camera specifications	CMOS camera	NIR camera
spectral range	350 – 1000 nm	900 – 1700 nm
sensor size	1024x1024 Pixel <sup>2</sup>	320x256 Pixel <sup>2</sup>
pixel size	10.6 $\mu\text{m}$	30 $\mu\text{m}$
frame rate (at full sensor size)	150 fps	~ 100 fps

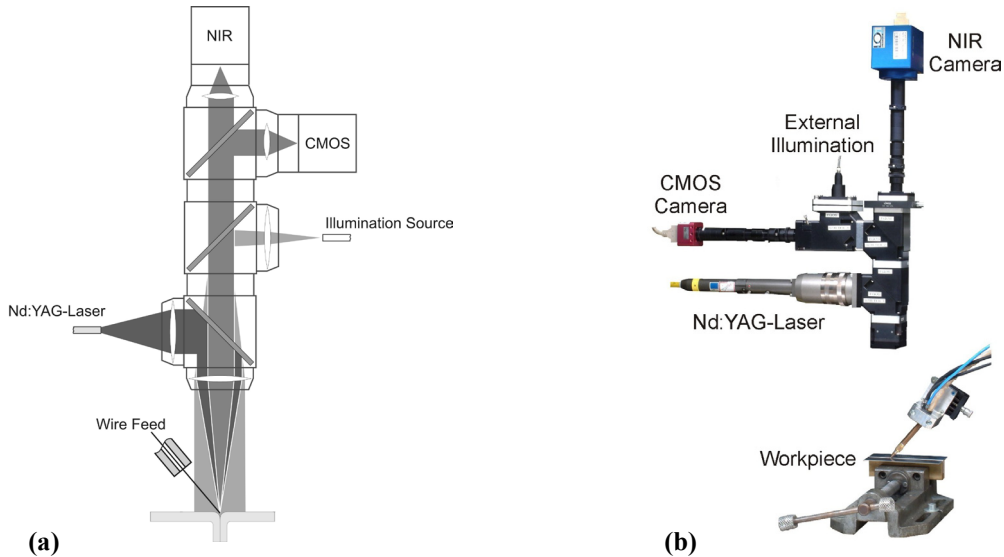


Figure 4: (a) Schematic sketch of the CPC system. (b) Realised system with two cameras and an external illumination.

### 3.2. Modification of the system

For the experiments described here the observation parameters have to be adapted. A pixel resolution of  $1024 \times 360$  pixels<sup>2</sup> is chosen for the CMOS camera while the exposure time is set to 0.5 ms. The NIR camera operates in a regime of 0.5 ms exposure time and  $320 \times 130$  pixels<sup>2</sup> special resolution. The frame rates are 350 fps and about 140 fps, respectively. With additional optical filters the spectral observation range of the NIR camera is set to 1200–1700 nm, while the CMOS camera captures in a narrow bandwidth around the centre wavelength of the external illumination source. In this case a diode laser with an output power of up to 20 W and a centre wavelength of 808 nm is chosen. It is also coaxially applied to the optical path of the CMOS camera. Size and shape of the illumination spot are adjusted in a way that it fits the field of view of the CMOS camera. As the magnification is roughly 1:1, the field of view of the camera is about  $10 \times 3.6$  mm<sup>2</sup>.

### 3.3. Detection capabilities of the CMOS camera

Fig. 5 (a) shows a typical image taken by the CMOS camera. In comparison to previous publications [3] the quality of the illumination is increased. One can clearly see the incoming brazing wire, the melt pool and the solidifying seam. Additionally, the surface of the ground material can be visualised good enough to run image processing algorithms for velocity detection, as will be discussed in Section 4.1. But also other process parameters like position and orientation of the solder wire or the dimension of the liquid phase can be determined by analysing these images taken by the CMOS camera. Also the surface of the solidified seam can be judged. Fig. 5 (b) gives an example of the appearance of the black jagged line described in Section 2. Hence, an indirect classification of the metallurgical composition of the seam could be possible.

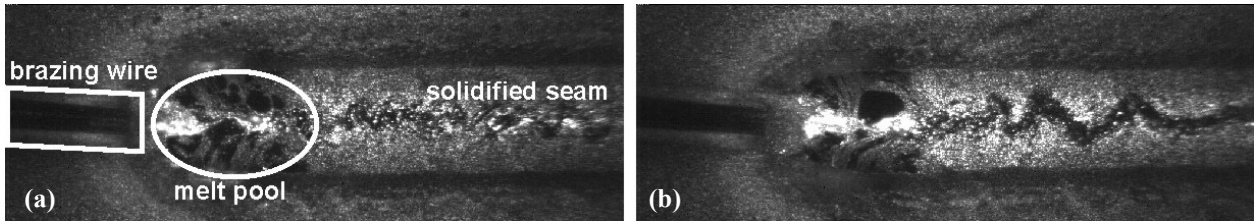


Figure 5: (a) Image of a normal brazing process taken by the CMOS camera and illuminated by the external illumination source. (b) Example of the some irregularities in the solidifying seam.

### 3.4. Detection capabilities of the NIR camera

In previous publications [3] the visualisation of pores has been already demonstrated. The visualisation of pores with a diameter less than  $200\ \mu\text{m}$  has been realised in the images taken by the NIR camera. In this section the detection of the other seam imperfections is investigated.

The thermal radiation of a process without any disturbance can be seen in Fig. 6 (a). The bright nearly round spot is the hottest area of the process zone. It is assumed that this area indicates the position where the laser beam hits the target. The thermal radiation of the joint partners – indicated through the long white tails reaching to the right – can be used to detect the seam boundaries.

On a first spot the thermal radiation of the process gives a good overview of the process symmetry. That enables a simple way of detecting the position of the lasers spot relative to the joint, as illustrated in Fig. 6 (a) and (b). In an experiment the laser is shifted by a lateral distance of  $0.2\ \text{mm}$  down its normal brazing position, to simulate a misalignment of the laser spot position. As the lower joint partner absorbs more energy of the incident laser beam the NIR camera detects an image with an asymmetrical heat distribution. In combination with the brazing wire position – detected in the images taken by the CMOS camera – the relative position between incoming brazing wire and the actual brazing spot can be measured and one can state, that the process conditions turn to a process condition with an increased probability of pore formation. In the worst case the spot of the brazing laser is that far misaligned that only the wetting of one joining partner is achieved. Hence, the proper seam creation is discontinued and a gap remains in the seam. This effect can also be detected by the thermal radiation as shown in Fig. 6 (d).

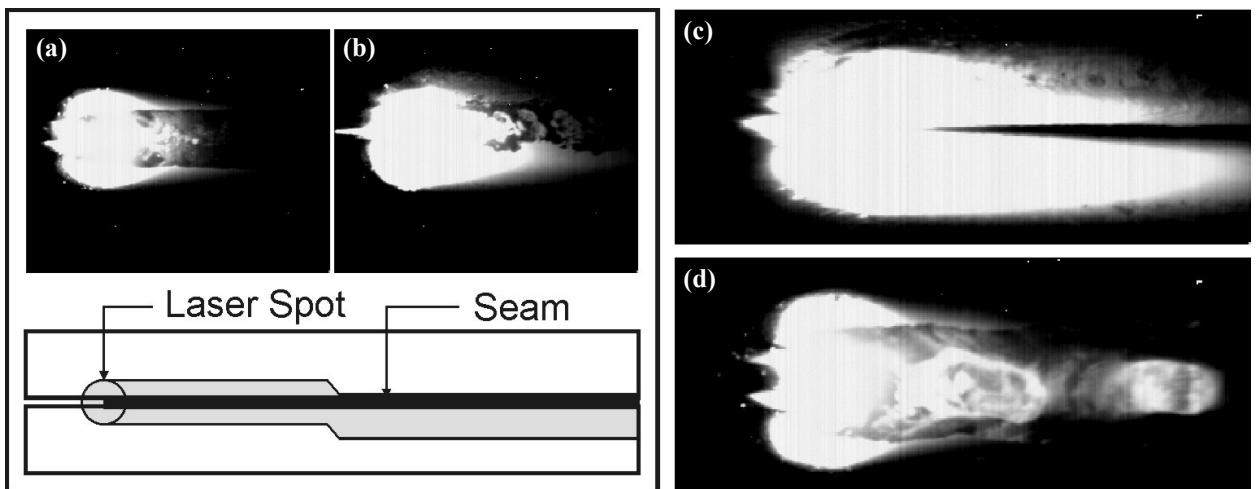


Figure 6: Overview of different process faults visualised by the NIR camera. (a) Standard brazing position. (b) Simulated misalignment of the laser spot position – the laser spot is shifted  $0.2\ \text{mm}$  down. (c) Image of a process with one side wetting behaviour. (d) Process where the brazing wire is not fully fused.

If there is not enough energy provided to the process the brazing wire cannot fully be fused. Some non fused pieces of the brazing wire remain in the solidified seam. Nevertheless these non fused pieces of brazing wire are still

hotter than the solidifying seam and can be observed in the images of the thermal radiation, see Fig. 7 (b). The non fused material spikes out of the seam surface and the roughness of the seam increases. The quality of the seam is therefore not acceptable.

#### 4. Monitoring of Process Parameters

In this section an overview of image processing algorithms for monitoring process parameters of the laser brazing process with respect to quality control is given.

##### 4.1. Brazing velocity

For determining the brazing velocity the fine-structured texture of the workpiece is utilized to apply a template matching algorithm (Fig. 5). Thus, the feed offset of the process between two consecutive frames in an image sequence taken by the CMOS camera can be obtained. For the template matching the normalized cross correlation (NCC) is used ([9], p.869-871). The cross correlation is defined by

$$c(x, y) = \sum_s \sum_t h(s, t) f(x + s, y + t) \quad (1)$$

where  $h$  is a  $m \times n$ -sized template and  $f$  denotes an image. The NCC is invariant to illumination changes which can occur in the process images (Fig. 5). The NCC is defined by

$$\gamma(x, y) = \frac{\sum_s \sum_t [h(s, t) - \bar{h}] \sum_s \sum_t [f(x + s, y + t) - \bar{f}(x + s, y + t)]}{\sqrt{\sum_s \sum_t [h(s, t) - \bar{h}]^2 \sum_s \sum_t [f(x + s, y + t) - \bar{f}(x + s, y + t)]^2}} \quad (2)$$

where  $\bar{h}$  is the mean value of the template  $h$  and  $\bar{f}$  is the mean value of the image.  $\gamma(x, y)$  has values in the range  $[-1, 1]$  and is invariant to variation of the absolute values of  $f$  and  $h$ . The maximum correlation  $\max(\gamma(x, y))$  is reached, when  $h$  and the corresponding region in  $f$  are identical.

For maintaining the feed offset a template of  $25 \times 25$  pixel<sup>2</sup> of the  $i$ -th image is matched in a search-area in the following  $(i+1)$ -th image of an image sequence. For saving calculation time the search-area is limited to an area close to the region of the template. The size of the search-area is specified by the size of the template, the maximum possible feed and an additional safety zone.

To gain more accuracy the NCC can be applied subpixel-wise by up scaling both, the template and the search-area.

After the feed offset is determined the process velocity can be calculated by

$$v = \frac{u * \alpha}{\beta} \quad (3)$$

where  $u$  denotes the feed offset,  $\alpha$  equates the frame rate of the CMOS camera and  $\beta$  is a constant which specifies the number of pixel per meter. An example for the determination of the brazing velocity over a whole video sequence of a brazing process is shown in Fig. 7.

The brazing velocity used for this sequence is 3.8 m/min and the determined brazing velocity between the start and the end of the process (frame 200 to 800) is about  $3.79 \pm 0.075$  m/min.

Another application for the calculated feed offset besides monitoring of the brazing velocity is creating an image mosaic for a whole brazed seam. As Fig. 8 illustrates, the mosaic is stitched together using only a part of an image which is always in the same image region and has a size defined by the feed offset. The seam mosaic can either be used for further analysis of the seam quality (with the benefit that the mosaic is homogeneously illuminated) or be archived for assurance purposes.

##### 4.2. Brazing time

The brazing time can be obtained by deriving it from the length of the melt pool which is delimited by the phase transitions from liquid to solid phase and vice versa. Thus, the feed offset of the process is utilized to detect the area of high dynamics, which equates the melt pool, by subtracting adjacent frames. The operational sequence of this

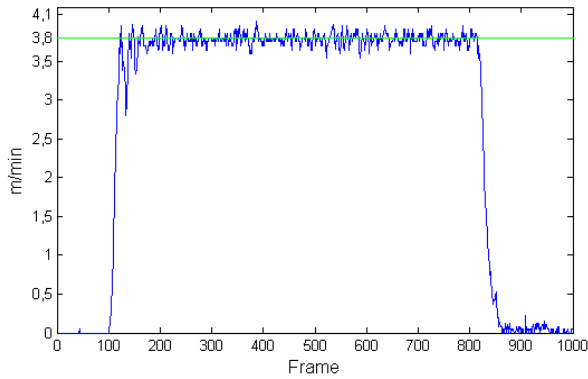


Figure 7: Determined brazing velocity over an image sequence of a brazing process with a speed of 3.8 m/min (marked by a green line)

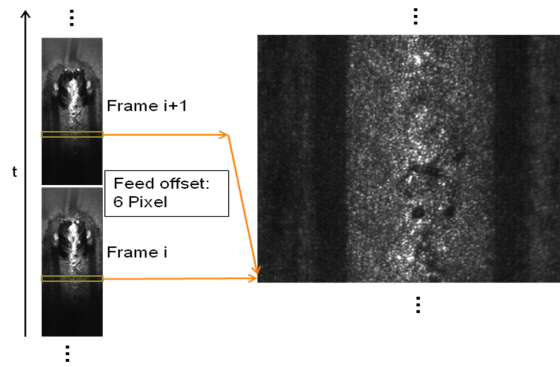


Figure 8: Mosaic stitching process with a part of a seam mosaic

procedure is shown in the block diagram in Fig. 9 The line by line calculation of the degree of dynamics can be formally described by

$$d(l) = |\max(I_i^T - I_{i+1}, l)| * |\min(I_i^T - I_{i+1}, l)| \quad (4)$$

where  $l$  is the image line,  $I$  stands for an image and  $T$  for the translation (Fig. 9).

The positions of the phase transitions can be obtained by segmenting the resulting elements of the vector  $d$  by

$$e(l) = \begin{cases} 1 & \text{if } d(l) \leq C, \\ 0 & \text{else.} \end{cases} \quad (5)$$

$C$  is a threshold separating the lines of high dynamics, which include the melt pool, from those of low dynamics affected by noise. The first line where the value exceeds the threshold is defined as the position of the phase transition from solid to liquid phase and the last line as the position of the phase transition from liquid to solid phase. The area of the melt pool is furthermore used to calculate the actual brazing time by

$$t_{bt} = \frac{L}{\beta * v} \quad (6)$$

In this formula  $L$  denotes the length of the melt pool area,  $v$  the brazing velocity and  $\beta$  signifies the number of pixel per meter. In Fig. 10 results for a set of brazing process sequences with different laser power settings are shown. The upper diagram shows for each power setting the mean value with its standard deviation for the two phase transitions. The lower diagram shows the mean value with its standard deviation for  $\bar{d}$  only within the determined melt pool area. The corresponding values for the brazing time which are calculated by (6) are  $60 \pm 43$  ms for the case where the laser power is set to 800 W (in this sequence nearly no wetting of the work piece occurred),  $171 \pm 5$  ms for the 1300 W case and  $230 \pm 8$  ms for the 1550 W case. The results show that the size of the melt pool, its dynamics and the corresponding brazing time are directly proportional to the laser output power.

### 4.3. Process geometry

Predications about the process geometry can be made by an analysis of the heat distribution for the area of high emission (AHE) in the NIR image. In order to segment the image into a binary image  $g$ , the following formula

$$g(x, y) = \begin{cases} 1 & \text{if } f(x, y) \leq k * \max(f), \\ 0 & \text{else.} \end{cases} \quad (7)$$

is used where  $k \in [0, \dots, 1]$ , yielding to a threshold by multiplying it with the maximum intensity value of the image  $\max(f)$ . Due to the fact that the image is clipped in the AHE, a high value for  $k$  is used (e.g.,  $k = 0.8$ ). In the resulting binary image the AHE object is the biggest connected component. For this object the global features area, centre of gravity (COG), orientation, bounding box, eccentricity and major axis length (MAL) are computed. As can

been seen in Fig. 11, the eccentricity of the AHE object decreases, the size of its area and MAL increases and the orientation and the COG changes for an asymmetric process. The detected asymmetry can indicate a lateral deviation of the laser spot from the joint which can lead to defects such as partial melting of the work piece and wetting failures.

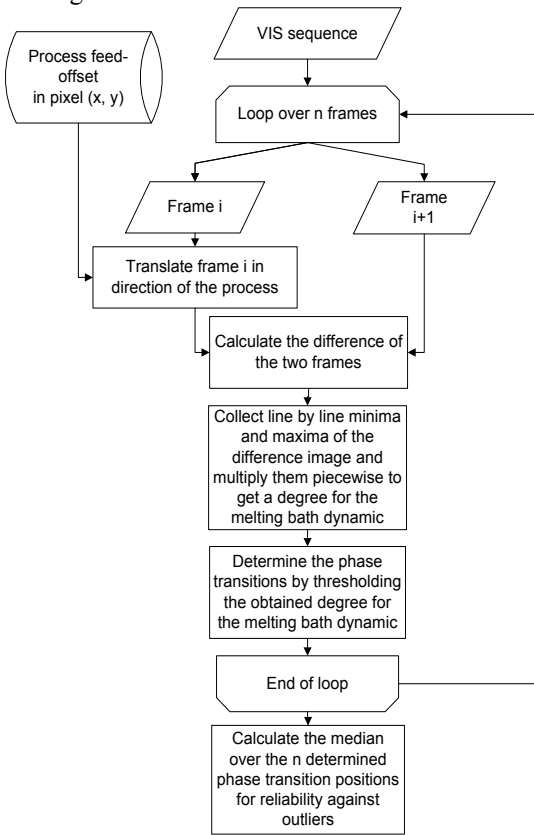


Figure 9: Block diagram of the procedure for detecting the size of the melting bath

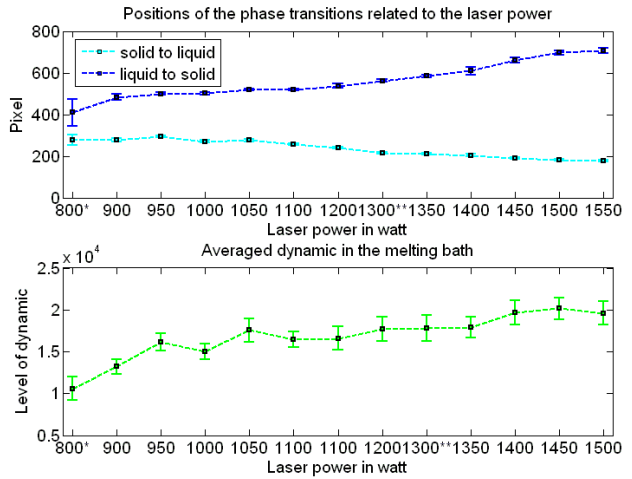


Figure 10: Results for a set of video sequences of brazing processes with a brazing velocity and a wire feed rate of 1.3 m/min and different laser power settings. \*: no wetting occurred \*\*: default value

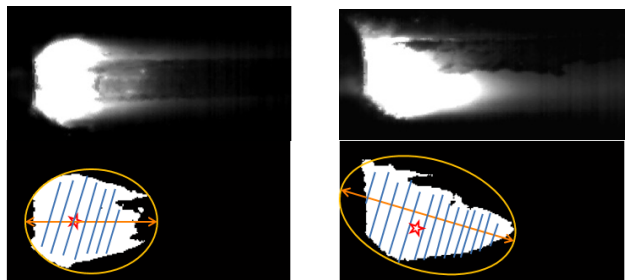


Figure 11: Output image and related binary image with marked features; (left) symmetric process, (right) asymmetric process

An additional task for the identification of the process geometry is the identification of the position and the orientation of the brazing wire in relation to the laser spot. Both values can be computed by a combined analysis of both images through image fusion on feature level. The relative position of the laser spot can be obtained from the AHE object in the NIR image. For this the horizontal position of its bounding box is used. The position and orientation of the brazing wire are determined by detecting it in the left region of the images taken by the CMOS camera, see Fig. 5. The brazing wire object is segmented in a similar way as in (7). As a difference, the threshold is calculated adaptively through the gray scale distribution because the solder object appears to be slightly darker than the surface of the work piece. Afterwards the bounding box and the orientation of the segmented brazing wire object are computed. The obtained position of the brazing wire object in the images taken by the CMOS camera is put into relation to the position of the AHE object in the NIR image. Hence the relative position of the brazing wire to the process is determined. As explained in section 2 this could be an approach to detect a critical process condition where the trigger probability of pore formation is increased.

## 5. Conclusion

It has been shown that different kinds of seam imperfections may occur during laser brazing. These were classified and divided into four basic types. In addition to those imperfections which mainly affect the seam geometry, two kinds of imperfections were identified that affect the metallurgical composition of the joint. The

formation mechanism of pores has been discussed. The findings regarding this mechanism have been partially verified by comparison to other groups. It has been shown that pores occur due to certain trigger events which disturb the wetting process. Process conditions which may facilitate such events have been identified and summarized. However, it is still impossible to predict the precise time and location at which a pore will occur. But there are some approaches of detecting these process conditions indirectly. This leads to the necessity of monitoring the brazing process by means of a suitable quality control system.

In its current stage of the development the optical system can resolve the geometrical dimensions of the process. Information that are necessary for the determination of process parameters like brazing velocity, melt pool length and the position of the brazing wire can be visualised by the CMOS camera in combination with an external illumination. In addition the images of the thermal radiation captured by the NIR camera turned out to be a useful tool for the detection of seam imperfections.

Based on the captured images image processing algorithms have been developed. Different process parameters can be measured to detect seam imperfections indirectly. In a next step seam imperfections will be detected directly from the images of the thermal radiation. Current works concentrates on image processing and pattern recognition algorithms for an automated on-line detection.

## Acknowledgements

The German Federal Ministry of Economics and Technology (BMWI, Project: IN7023-EQOS) is gratefully acknowledged for financial support of the project “Development and Qualification of a simple On-line Quality Monitoring System for the industrial Laser Brazing“

## References

1. U. Müßigmann, J. Schwarz, J. Kubon: Qualitätsprüfung an Laserlöt- und Laserschweißnähten. *Horizonte* 23, pp. 20-22, December 2003.
2. J. Müller-Borhanian, M. Halschka: Schweiß- und Löt­nähte automatisch überwacht – Praxisbeispiele belegen die Funktionalität bei Laserapplikationen. *Laser Technik Journal*, 5, Nr. 5, pp. 40-42, 2008.
3. A. Grimm, M. Schmidt: Possibilities for online process monitoring at laser brazing based on two dimensional detector systems. ICALEO 2009, Proc. 28<sup>th</sup> Int. Congr. on Applications of Laser & Electro Optics, Orlando, FL, USA, 2009.
4. G. Humpston, D. M. Jacobson: Principles of Soldering and Brazing. ASM International, Materials Park, OH, USA, 1993, ISBN 0-87170-462-5.
5. Donst, D. et al: On-line quality control system for laser brazing. ICALEO 2009, Proc. 28<sup>th</sup> Int. Congr. on Applications of Laser & Electro Optics, Orlando, FL, USA, 2009.
6. Kimura, S. et al.: Laser brazing phenomena of galvanized steel and pit formation mechanism. ICALEO 2006, Proc. 25<sup>th</sup> Int. Congr. on Applications of Laser & Electro Optics, Scottsdale, AZ, USA, 2006.
7. Kaierle, S.; P. Abels; Fiedler, W.; Mann, S.; Regaard, B.: Online-Qualitätssicherung für das Laserstrahlschweißen. *MB-Revue* – 2008, pp. 132-135, 2008.
8. Kaierle, S.: Process monitoring and control of laser beam welding. *Laser Technik Journal*, 5, Nr.3, pp. 41-43, 2008.
9. R. C. Gonzalez and R. E. Woods, *Digital Image Processing* 3. ed., Upper Saddle River, NJ, Pearson Prentice Hall, 2008.